

CP(N−1) Quantum Field Theories with Alkaline-Earth Atoms in Optical Lattices

C. Laflamme^{1,2}, W. Evans³, M. Dalmonte^{1,2}, U. Gerber⁴, H. Mejía-Díaz⁴, W. Bietenholz⁴, U.-J. Wiese³, P. Zoller^{1,2}

¹ Institute for Theoretical Physics, University of Innsbruck, A-6020, Innsbruck, Austria

² Institute for Quantum Optics and Quantum Information, Austrian Academy of Sciences, A-6020, Innsbruck, Austria

³ Albert Einstein Center, Institute for Theoretical Physics, Bern University, 3012 Bern, Switzerland

⁴ Instituto de Ciencias Nucleares, Universidad Nacional Autónoma de México, A.P. 70-53, C.P. 04510 Distrito Federal, Mexico

(Dated: July 27, 2015)

We propose a cold atom implementation to attain the continuum limit of (1+1)-d CP(N−1) quantum field theories. These theories share important features with (3+1)-d QCD, such as asymptotic freedom and θ vacua. Moreover, their continuum limit can be accessed via the mechanism of dimensional reduction. In our scheme, the CP(N−1) degrees of freedom emerge at low energies from a ladder system of SU(N) quantum spins, where the N spin states are embodied by the nuclear Zeeman states of alkaline-earth atoms, trapped in an optical lattice. Based on Monte Carlo results, we establish that the continuum limit can be demonstrated by an atomic quantum simulation by employing the feature of asymptotic freedom. We discuss a protocol for the adiabatic state preparation of the ground state of the system, the real-time evolution of a false θ -vacuum state after a quench, and we propose experiments to unravel the phase diagram at non-zero density.

PACS numbers: 67.85d, 11.15.Ha, 37.10.Vz, 75.10.Jm

Recently, there has been growing interest in developing physical platforms for quantum simulation of Abelian and non-Abelian gauge theories [1–9]. This effort is motivated by applications in particle and condensed matter physics, with the hope of developing quantum simulation [10] as a new tool to access regimes and phenomena complementary to, and beyond, classical simulations [2]. Previous work has focused on implementing quantum simulation of *lattice* gauge theories. An outstanding example is provided by cold atoms in optical lattices as a natural and controlled environment [10], where the lattice gauge theory of interest emerges as a low-energy effective description of tailored atomic Hubbard dynamics [2, 7]. Applications in particle physics, however, ultimately require taking the *continuum limit*, to eliminate artifacts due to the discretization of space.

While some effective field theories emerge directly from cold atom systems in free space, here we construct lattice field theories from atoms in an optical lattice. Then, instead of following the standard procedure of Wilson’s lattice theory, where the continuum limit is approached by tuning a bare coupling constant [11], we use the formalism of D-theory, in which the continuum limit emerges via dimensional reduction [12, 13].

We illustrate this idea for the relevant example of CP(N−1) quantum field theories [14, 15]. Such models have attracted interest in the context of particle physics as toy models for QCD, with which they share key features such as asymptotic freedom, the nonperturbative generation of a mass gap, and the existence of nontrivial θ -vacua [14, 15]. In addition, in a condensed matter context CP(N−1) models [16] have recently been discussed in relation to deconfined quantum criticality [17, 18]. As discussed below, the CP(N−1) model in (1+1)-d

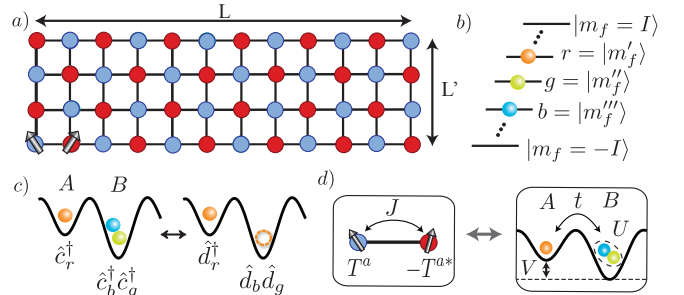


FIG. 1. a) Atomic setup for the implementation of the CP(N−1) model, where SU(N) spins are arranged on a 2D bipartite spatial lattice of volume $L \times L'$ with $L \gg L'$. b) The N spin states are realized by AEAs occupying $N \leq 2I + 1$ hyperfine states, where I is the nuclear spin, with Zeeman splitting due to a uniform magnetic field. c) Identifying $c^\dagger \leftrightarrow d^\dagger$ (cf. Eqs. (5) and (6)) on sublattice A, and $c^\dagger \leftrightarrow d$ on sublattice B, gives rise to the description of SU(N) spins in the fundamental (red/dark), and anti-fundamental representation (blue/light), respectively, with 1 and $N - 1$ fermions per site. d) Interactions between SU(N) spin T^a and $-T^{a*}$ are generated via superexchange, where $J \propto t^2/U$. An energy offset V allows for full tunability of J.

emerges via dimensional reduction as the effective low-energy dynamics of certain (2+1)-d spin ladder models of SU(N) quantum magnetism. These SU(N) quantum spin models have a natural, and realistic implementation with fermionic Alkaline Earth Atoms (AEAs) [19–31].

The SU(N) spin model of interest, and the corresponding atomic setup are illustrated in Fig. 1. We assume fermionic AEAs with nuclear spin I representing SU(N) spins with $N \leq 2I + 1$. These atoms are loaded into a bipartite 2D spatial lattice of volume $L \times L'$ ($L \gg L'$), realized as an optical superlattice. The lattice depths and the

interactions between the atoms are adjusted to achieve a filling with 1 and $N - 1$ atoms on the A and B sites of the bipartite lattice, respectively. Atoms on neighboring sites will then interact via superexchange processes. In our discussion we will first provide a detailed description of the $SU(N)$ spin model and its dimensional reduction to the $(1 + 1)$ -d $\mathbb{CP}(N - 1)$ model, and then proceed to details of the atomic physics implementation. We emphasize that recent atomic physics experiments have demonstrated the basic ingredients of our setup. Equally important, the most prominent many-body aspects of the model, such as asymptotic freedom and the effect of the θ -term, can be probed using well-established techniques such as noise correlations and band mapping.

Model Hamiltonian.— The quantum spin models are described by the Hamiltonian

$$H = -J \sum_{\langle xy \rangle, x \in A} T_x^a T_y^{a*}, \quad J > 0, \quad (1)$$

where T_x^a and $-T_y^{a*}$ are generalized spin operators transforming under the fundamental and anti-fundamental representation of $SU(N)$, residing on sites $x \in A$ and $y \in B$ of the even and odd sublattices, respectively. This particular selection of the spin representation, as well as the antiferromagnetic $J > 0$ requirement, are vital to obtain the $\mathbb{CP}(N - 1)$ model in the continuum limit. The spin operators satisfy $[T_x^a, T_y^b] = i\delta_{xy} f_{abc} T_x^c$, where f_{abc} are the structure constants of $SU(N)$. Note that the $N = 2$ case of Eq. (1) reduces to the Heisenberg model. The system has a global $SU(N)$ symmetry with total spin conservation,

$$[H, T^a] = \left[H, \sum_{x \in A} T_x^a - \sum_{y \in B} T_y^{a*} \right] = 0. \quad (2)$$

We now illustrate the method of dimensional reduction to obtain the $\mathbb{CP}(N - 1)$ model from Eq. (1). For $N = 3, 4$, in the zero-temperature thermodynamic limit $L, L' \rightarrow \infty$, the $SU(N)$ symmetry breaks spontaneously down to $U(N - 1)$ [32], resulting in $2(N - 1)$ massless Nambu-Goldstone bosons described by fields in the coset space $SU(N)/U(N - 1) = \mathbb{CP}(N - 1)$. These can be described by $N \times N$ Hermitian projection matrices P , with $\text{Tr} P = 1, P^2 = P$ and $P^\dagger = P$. In the case of a finite extent L' , as a result of the Mermin-Wagner theorem, massless Nambu-Goldstone bosons are forbidden; they pick up a mass $m = 1/\xi$, where ξ is the correlation length. Due to asymptotic freedom of the $(1 + 1)$ -d $\mathbb{CP}(N - 1)$ model, ξ grows exponentially with L' ,

$$\xi \propto \exp(4\pi L' \rho_s / (cN)) \gg L'. \quad (3)$$

Here ρ_s is the spin stiffness parameter and c is the spin-wave velocity. As L' increases, ξ becomes much larger than L' and thus the system undergoes dimensional reduction. It is then described by the effective action [33]

$$S[P] = \frac{1}{g^2} \int d^2x \text{Tr} \left[\partial_x P \partial_x P + \frac{1}{c^2} \partial_t P \partial_t P \right] - i\theta Q[P], \quad (4)$$

where $Q[P] \in \Pi_2[\mathbb{CP}(N - 1)] = \mathbb{Z}$ is the topological charge, and $g^2 = c/(L' \rho_s)$ is the coupling constant of the dimensionally reduced theory. The vacuum angle is given by $\theta = n\pi$ [33], where $n = L'/a$ is the number of legs in the L' direction, and a is the lattice spacing. For $N = 2$ this reduces to the well-known $O(3)$ field theory description of the low-energy physics in Heisenberg antiferromagnets. In contrast to Wilson's lattice field theory, in D-theory [34] the continuum limit, $\xi/a \rightarrow \infty$, is approached by increasing L' , not by decreasing a bare coupling constant. Due to the exponential dependence of ξ on $L' = na$, cf. Eq. (3), the continuum limit is already reached for moderate values of L' , which are accessible in current experiments. This strategy to regularize strongly coupled field theories is generally employed in the context of D-theory: in particular, in the D-theory regularization of QCD (3+1)-d gluon fields arise from dimensional reduction as collective excitations of (4+1)-d $SU(3)$ quantum links, while chiral quarks arise as domain wall fermions [12].

Implementation with AEAs.— The Hamiltonian (1) is realized in a natural way in a system of AEAs trapped in an optical lattice, based on their inherent $SU(N)$ symmetry [21]. Our implementation conceptually rests on two main ideas: first, formulating the Hamiltonian (1) in terms of fermionic degrees of freedom, and second, implementing a particle-hole transformation to account for the fundamental/anti-fundamental representation of $SU(N)$ spins with $N \geq 3$. In practice, this implementation exploits the toolbox already demonstrated in systems of trapped AEAs [19–30].

We first rewrite the spins in Hamiltonian (1) as fermion bilinears

$$T_x^a = \sum_{mm'} d_{xm}^\dagger \lambda_{mm'}^a d_{xm'}, \quad -T_x^{a*} = - \sum_{mm'} d_{xm}^\dagger \lambda_{mm'}^{a*} d_{xm'}, \quad (5)$$

where λ^a are the generalized Gell-Mann matrices, $\text{Tr}[\lambda^a \lambda^b] = 2\delta^{ab}$, and d_{xm} annihilates a fermionic mode at position x , with the indices $m, m' \in \{1, \dots, N\}$ labelling N generic states. In this way, the spin Hamiltonian is formulated in terms of fermionic degrees of freedom.

Next, we turn to a system of fermionic AEAs trapped in a 2D bipartite optical lattice, cf. Fig. 1.a). We assume the $2I + 1$ nuclear spin states to be split in energy due to a uniform magnetic field (Fig. 1.b)). The Hamiltonian of such a system is expressed in terms of localized Wannier functions [21] as

$$\begin{aligned} H &= H_t + H_U, \\ H_t &= -t \sum_m \sum_{\langle xy \rangle} (c_{xm}^\dagger c_{ym} + c_{ym}^\dagger c_{xm}) \\ H_U &= \frac{U}{2} \sum_x n_x (n_x - 1) + V \sum_{x \in A} n_x. \end{aligned} \quad (6)$$

Here, c_{xm} is the annihilation operator for an atom with

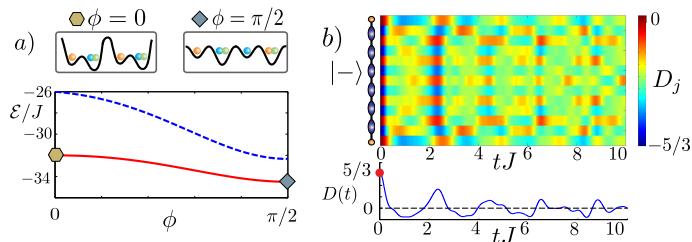


FIG. 2. a) Energy of the ground state (red, solid) and excited state (blue, dashed), in units of the spin coupling J , as a function of the adiabatic parameter $\tau = \sin \phi$. Schematics show the evolution of the system from $\phi = 0$ (bottom left) to $\phi = \pi/2$ (top right). b) Time evolution of the false vacuum state for a 14 site system. Upper panel: Order parameter calculated at each bond as a function of time. Lower Panel: Time evolution of the order parameter summed over all bonds (see text).

nuclear spin $m \in \{-I, \dots, I\}$ in the Wannier function localized at site x , and $n_x = \sum_m c_{xm}^\dagger c_{xm}$ is the corresponding particle number operator. We denote by t the nearest-neighbor hopping amplitude, U is an onsite interaction energy, and V is an energy offset between the two sublattices. Since the scattering length is independent of the nuclear spin level m , the system of AEAs has a global $SU(2I+1)$ symmetry. Note that one can take $N \leq 2I+1$ by initializing atoms into a subset of the magnetic states; if states are initially empty, the symmetry ensures that they will remain so. AEAs can realize $SU(N)$ physics up to $N = 10$ (e.g. ^{87}Sr and ^{173}Yb), but here we will concentrate on the $\mathbb{CP}(2)$ model, i.e. $N = 3$, since it is particularly interesting from a theoretical viewpoint.

We initially occupy each site of the A sublattice with 1, and each site of the B sublattice with $N - 1$ atoms. While the A sublattice spins in the fundamental representation of $SU(N)$ are embodied by a single fermion, the B sublattice spins in the anti-fundamental representation are embodied by $N - 1$ fermions, which are equivalent to a single hole, cf. Fig. 1.c). Using the fermionic representation of Eq. (5), we identify c_x with d_x on sublattice A , and with d_x^\dagger on sublattice B .

We now consider the Hamiltonian (6) in the strong coupling regime, $t \ll U, V$: the contribution of H_t causes virtual tunneling processes within the subspace of states with fixed particle numbers per site (the eigenstates of H_U), thus generating $SU(N)$ superexchange terms [30]. In this regime, to second order in t/U the Hamiltonian (1) emerges with [16]

$$J = \frac{t^2 U}{(-V + U(N - 3))(V - U(N - 1))}, \quad (7)$$

where an antiferromagnet requires $J > 0$.

The ground state of the system can be prepared via an adiabatic protocol: we start by preparing a band insulator with N particles per site on a simple square lattice.

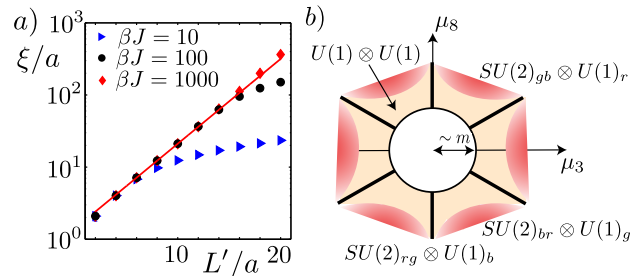


FIG. 3. Panel a): Results from Monte Carlo simulations for $\mu_3 = \mu_8 = 0$, at $\beta J = 10$ (blue triangles), $\beta J = 100$ (black circles) and $\beta J = 1000$ (red diamonds) for the correlation length ξ in the long L -direction, with $L = 1500a$. Error bars are too small to be seen. The best fit line for $\beta J = 1000$, $\xi/a = 1.22157 \cdot \exp[0.270784 L'/a]$, is obtained using the range $4 < L'/a < 12$ — at smaller values of L' the system is subject to significant finite size effects, while at larger values of L' the system size L becomes comparable to ξ . Panel b): Conjectured phase diagram of $\mathbb{CP}(2)$ models as a function of the chemical potentials μ_3, μ_8 . In the vicinity of $\mu_3 = \mu_8 = 0$, the ground state is the vacuum. Besides a normal fluid phase (yellow), high density color superfluid phases (red) are expected to appear. The phase diagram can be explored in the proposed cold atom setup.

The population in each spin state can be precisely controlled using, e.g. optical pumping [29, 30]. Each site is subsequently split into a double well by adiabatically ramping up a superlattice, realizing a system of generalized $SU(N)$ singlets akin to what has already been realized using bosonic alkali atoms [35]. The barrier between the wells is then adiabatically turned off, thus realizing the full quantum dynamics of Eq. (1). This procedure relies entirely on existing techniques, and can be applied for $N = 3, 4$ and various L' . For a single chain this works as follows: starting from a perfectly dimerized initial state, the inter-well exchange is switched on according to the time-dependent Hamiltonian

$$H(\tau) = -(1 - \tau)J \sum_{x \in A} T_x^a T_{x+\hat{1}}^{a*} + \tau H, \quad (8)$$

where $\tau \in [0, 1]$ is the adiabatic parameter. The corresponding low-lying spectrum of a 14 site system is shown in Fig. 2. One does not cross a phase transition during this process; the gap does not close while changing τ from 0 to 1 [36]. This ensures that an adiabatic ramp can be performed on timescales much shorter than $1/J$.

Continuum Limit. —In order to demonstrate explicitly that the $SU(3)$ spin ladder gives rise to the $\mathbb{CP}(2)$ model in the continuum limit, it is vital to study the correlation length and verify that it increases exponentially with the size L' of the extra dimension, see Eq. (3). By means of Monte Carlo simulations with a loop cluster algorithm [37] we have calculated the spatial correlation length ξ [38]. For even L' we obtain Fig. 3.a), which indeed shows the anticipated exponential increase of ξ

with L' , in agreement with asymptotic freedom of the $\text{CP}(2)$ model that emerges via dimensional reduction. The increase of the correlation length for $L'/a = 4$ to 12 should already be accessible using current experimental techniques. Even at temperatures around $\beta J \sim 10$, corresponding to a physical temperature on the order of $\sim \text{nK}$, the correlation length $\xi(6a)$ is close to $10a$, and already falls on the exponential that indicates asymptotic freedom. The correlation length ξ can be measured in a cold atoms setup via Bragg spectroscopy or through noise correlations [10].

Finite Density Phase Diagram.—Just like QCD, $\text{CP}(N-1)$ models have a finite density phase diagram that is worth exploring. While in QCD a chemical potential μ can be coupled to the baryon number, in the $\text{CP}(2)$ model two chemical potentials, μ_3 and μ_8 , can be coupled to the global $\text{SU}(3)$ symmetry, which is thereby explicitly broken down to $\text{U}(1) \times \text{U}(1)$, or to $\text{SU}(2) \times \text{U}(1)$ along the solid lines in Fig. 3.b). It is then interesting to ask whether the $\text{U}(1)$ symmetries are affected by Kosterlitz-Thouless (KT) transitions. In a cold atom experiment a finite density situation is generated by loading the optical lattice with unequal numbers of atoms in the three Zeeman states. A KT transition is then signaled by the ‘condensation’ of bosonic molecules, formed from two fermions in specific combinations of Zeeman states, in the sense of color superfluidity [39–41].

C-breaking at $\theta = \pi$.—Having advocated the feasibility of approaching the continuum limit in a quantum simulation, we now consider an odd number n of transversely coupled chains, corresponding to $\theta = \pi$. At this point, analytical considerations suggest a first order phase transition with spontaneous charge conjugation (C) symmetry breaking [42], which has since been confirmed numerically [33]. In our proposed experimental realization with discrete spins, C corresponds to a shift in the longitudinal 1-direction, $T_x^a \rightarrow -T_{x+\hat{1}}^{a*}$, $-T_x^{a*} \rightarrow T_{x+\hat{1}}^a$, where the sites x and $x + \hat{1}$ belong to the A and B sublattice, respectively. An order parameter which signals C breaking in spin systems is given by [43]

$$D = \sum_{x \in A} \langle T_x^a T_{x+\hat{1}}^{a*} - T_x^a T_{x-\hat{1}}^{a*} \rangle, \quad (9)$$

which, equivalently, detects dimerization. When C is preserved (n even, $\theta = 0$) D vanishes, whereas when it is spontaneously broken (n odd, $\theta = \pi$) there are two degenerate ground states with opposite non-zero values of D , cf. Fig. 4. In a cold atom setup, measuring the singlets contributing to D has been proposed and demonstrated via spin changing collisions [10, 44]. A possible adiabatic preparation scheme for the realization of such generalized resonating valence bond states is illustrated in Fig. 2.a).

Quench Dynamics Decay of a False Vacuum.—The possibility of initializing states composed of singlets provides an opportunity to investigate real-time quenched

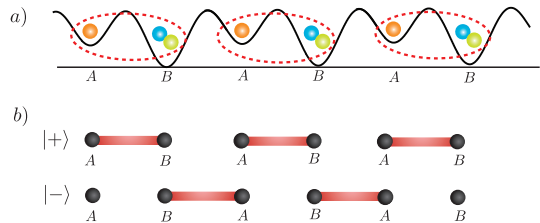


FIG. 4. Symmetry of the ground states for $\theta = \pi$. a) In the ground state bonds emerge between two neighboring sites on sublattice A and B . The ordering of the bonds gives rise to a double degeneracy of the ground state. b) Cartoon of the two degenerate ground states. A solid line indicates a dominant $\langle T_x^a T_{x+\hat{1}}^{a*} \rangle$, while no line represents a smaller value.

dynamics driven by H . In a finite system with open boundary conditions and even L , one can investigate how a false vacuum $|-\rangle$, cf. Fig. 4.b), decays as a function of time after the Hamiltonian H is switched on. Such a false vacuum decay can mimic processes in inflationary early universe cosmology, as well as bubble nucleation at a first order phase transition. Due to energy conservation the false vacuum, which has an energy cost for any finite system size L , cannot decay fully into the true vacuum $|+\rangle$. Instead one expects damped coherent oscillations between the two vacuum states. In order to quantify the false vacuum decay in real time, for a single chain we consider the order parameter $D(t) = \sum_{x \in A} \langle \Psi(t) | (T_x^a T_{x+\hat{1}}^{a*} - T_x^a T_{x-\hat{1}}^{a*}) | \Psi(t) \rangle$ which indicates whether singlet states predominantly form on the even or odd bonds. This order parameter is maximal for $|-\rangle$ (all even bonds have a singlet). In Fig. 2.b), we show the dynamics of the false vacuum decay evaluated by exact diagonalization of a $L/a = 14$ site system starting in the initial state $|-\rangle$. At times $tJ \ll 1$ the even singlets (blue) are stable. At later times, the false vacuum decays, with correlations remaining only in the central part of the system, while the bonds close to the boundary revert the order. The decay of the full order parameter is depicted in the lower panel, which indeed shows coherent oscillations. Both the order parameter and the local singlet projectors can be experimentally measured as discussed in the previous section. While moderate system sizes can be reached using exact diagonalization, the real-time dynamics in the continuum limit is inaccessible to classical simulations. Experiments using the present scheme would shed light on the real-time dynamics of false vacua in $\text{CP}(N-1)$ models.

Conclusions.—We have outlined a proposal for the quantum simulation of a $\text{CP}(N-1)$ quantum field theory using cold atoms trapped in an optical lattice with a ladder geometry. Our work shows how the continuum limit can be assessed using dimensional reduction, and how paradigmatic phenomena such as asymptotic freedom can be observed in cold atom experiments. Extending such investigations to non-Abelian gauge theo-

ries could provide an indispensable tool for the quantum simulation of fundamental theories such as QCD at finite baryon density. Moreover, the present scheme can also be extended to investigate condensed matter inspired $SU(N)$ models using alternating representations, relevant for (1+1)-d and (2+1)-d quantum magnets, and discussed in the context of deconfined quantum criticality [18].

Acknowledgments. We thank D. Banerjee, L. Fallani, C.V. Kraus, M. Punk, E. Rico, and S. Sachdev for useful discussions. This work was supported by the Schweizerischer Nationalfonds, the European Research Council by means of the European Union's Seventh Framework Programme (FP7/2007-2013)/ERC grant agreement 339220, the Mexican Consejo Nacional de Ciencia y Tecnología (CONACYT) through project 155905/10 and by DGAPA-UNAM, grant IN107915. Work in Innsbruck is partially supported by the ERC Synergy Grant UQUAM, SIQS, and the SFB FoQuS (FWF Project No. F4016-N23). CL was partially supported by NSERC.

-
- [1] D. Banerjee, M. Dalmonte, M. Müller, E. Rico, P. Stebler, U.-J. Wiese, and P. Zoller, *Phys. Rev. Lett.* **109**, 175302 (2012).
- [2] U.-J. Wiese, *Ann. Phys.* **525**, 777 (2013).
- [3] D. Banerjee, M. Bögli, M. Dalmonte, E. Rico, P. Stebler, U.-J. Wiese, and P. Zoller, *Phys. Rev. Lett.* **110**, 125303 (2013).
- [4] E. Zohar, J. I. Cirac, and B. Reznik, *Phys. Rev. Lett.* **110**, 125304 (2013).
- [5] L. Tagliacozzo, A. Celi, A. Zamora, and M. Lewenstein, *Ann. Phys.* **330**, 160 (2013).
- [6] K. Stannigel, P. Hauke, D. Marcos, M. Hafezi, S. Diehl, M. Dalmonte, and P. Zoller, *Phys. Rev. Lett.* **112**, 120406 (2014).
- [7] E. Zohar, J. I. Cirac, and B. Reznik (2015), arXiv:1503.02312.
- [8] S. Notarnicola, E. Ercolessi, P. Facchi, G. Marmo, S. Pascazio, and F. V. Pepe, *J. Phys. A* **48**, 30FT01 (2015).
- [9] A. Bazavov, Y. Meurice, S.-W. Tsai, J. Unmuth-Yockey, and J. Zhang (2015), arXiv:1503.08354.
- [10] I. Bloch, J. Dalibard, and S. Nascimbène, *Nat. Phys.* **8**, 267 (2012).
- [11] K. G. Wilson, *Phys. Rev. D* **10**, 2445 (1974).
- [12] R. Brower, S. Chandrasekharan, and U.-J. Wiese, *Phys. Rev. D* **60**, 094502 (1999).
- [13] R. Brower, S. Chandrasekharan, S. Riederer, and U.-J. Wiese, *Nucl. Phys. B* **693**, 149 (2004).
- [14] A. D'Adda, M. Lüscher, and P. Di Vecchia, *Nucl. Phys. B* **146**, 63 (1978).
- [15] H. Eichenherr, *Nucl. Phys. B* **146**, 215 (1978).
- [16] A. Auerbach, *Interacting Electrons and Quantum Magnetism* (Springer, 1994).
- [17] R. K. Kaul and A. Sandvik, *Phys. Rev. Lett.* **108**, 137 (2012).
- [18] R. K. Kaul and M. Block (2015), arXiv:1502.05128.
- [19] T. Fukuhara, Y. Takasu, M. Kumakura, and Y. Takahashi, *Phys. Rev. Lett.* **98**, 030401 (2007).
- [20] M. A. Cazalilla, A. F. Ho, and M. Ueda (2009), arXiv:0905.4948.
- [21] A. V. Gorshkov, M. Hermele, V. Gurarie, C. Xu, P. Julienne, J. Ye, P. Zoller, E. Demler, M. D. Lukin, and A. M. Rey, *Nat. Phys.* **6**, 289 (2010).
- [22] B. J. DeSalvo, M. Yan, P. G. Mickelson, Y. N. Martinez de Escobar, and T. C. Killian, *Phys. Rev. Lett.* **105**, 030402 (2010).
- [23] S. Stellmer, M. K. Tey, B. Huang, R. Grimm, and F. Schreck, *Phys. Rev. Lett.* **103**, 200401 (2009).
- [24] S. Stellmer, R. Grimm, and F. Schreck, *Phys. Rev. A* **84**, 043611 (2011).
- [25] S. Sugawa, K. Inaba, S. Taie, R. Yamazaki, M. Yamashita, and Y. Takahashi, *Nat. Phys.* **7**, 642 (2011).
- [26] M. D. Swallows, M. Bishof, Y. Lin, S. Blatt, M. J. Martin, A. M. Rey, and J. Ye, *Science* **331**, 1043 (2011).
- [27] S. Taie, R. Yamazaki, S. Sugawa, and Y. Takahashi, *Nat. Phys.* **8**, 825 (2012).
- [28] X. Zhang, M. Bishof, S. L. Bromley, C. V. Kraus, M. S. Safronova, P. Zoller, A. M. Rey, and J. Ye, *Science* **345**, 1467 (2014).
- [29] G. Pagano, M. Mancini, G. Cappellini, P. Lombardi, F. Schäfer, H. Hu, X.-J. Lio, J. Catani, C. Sias, M. Inguscio, et al., *Nat. Phys.* **10**, 198 (2014).
- [30] F. Scazza, C. Hofrichter, M. Höfer, P. C. De Groot, I. Bloch, and S. Fölling, *Nat. Phys.* **10**, 779 (2014).
- [31] G. Cappellini, M. Mancini, G. Pagano, P. Lombardi, L. Livi, M. Siciliani de Cumis, P. Cancio, M. Pizzocaro, D. Calonico, F. Levi, et al., *Phys. Rev. Lett.* **113** (2014).
- [32] K. Harada, N. Kawashima, and M. Troyer, *Phys. Rev. Lett.* **90**, 117203 (2003).
- [33] B. B. Beard, M. Pepe, S. Riederer, and U.-J. Wiese, *Phys. Rev. Lett.* **94**, 010603 (2005).
- [34] U.-J. Wiese, *PoS LAT2005* **281** (2005).
- [35] S. Nascimbène, Y.-A. Chen, M. Atala, M. Aidelsburger, S. Trotzky, B. Paredes, and I. Bloch, *Phys. Rev. Lett.* **108**, 205301 (2012).
- [36] We have numerically checked that the gap remains of order $0.6J$ even at $L = 60$.
- [37] N. Kawashima and K. Harada, *JPSJ* **73**, 1379 (2004).
- [38] The Monte Carlo simulations were performed with periodic boundary conditions in the L direction, and open boundary conditions in the L' direction. The correlation length ξ and second moment correlation length ξ_2 are measured and compared to ensure that the difference is negligible.
- [39] K. Rajagopal and F. Wilczek, *At the frontier of particle physics: Handbook of QCD* (World Scientific Singapore, 2001).
- [40] Á. Rapp, G. Zarand, C. Honerkamp, and W. Hofstetter, *Phys. Rev. Lett.* **98**, 160405 (2007).
- [41] A. Kantian, M. Dalmonte, S. Diehl, W. Hofstetter, P. Zoller, and A. J. Daley, *Phys. Rev. Lett.* **103**, 240401 (2009).
- [42] N. Seiberg, *Phys. Rev. Lett.* **53**, 637 (1984).
- [43] N. Read and S. Sachdev, *Phys. Rev. Lett.* **62**, 1694 (1989).
- [44] B. Paredes and I. Bloch, *Phys. Rev. A* **77**, 023603 (2008).